Temperature-dependent symmetry energy of neutron-rich thermally fissile nuclei

Abdul Quddus,[1] M. Bhuyan,[2,3,4] Shakeb Ahmad,[1] B. V. Carlson,[4] and S. K. Patra[5,6]
[1]*Department of Physics, Aligarh Muslim University, Aligarh 202002, India*
[2]*Department of Physics, Faculty of Science, University of Malaya, Kuala Lumpur 50603, Malaysia*
[3]*Institute of Research and Development, Duy Tan University, Da Nang 550000, Vietnam*
[4]*Instituto Tecnológico de Aeronáutica, 12.228-900 São José dos Campos, São Paulo, Brazil*
[5]*Institute of Physics, Bhubaneswar 751005, India*
[6]*Homi Bhabha National Institute, Training School Complex, Anushakti Nagar, Mumbai 400085, India*

(Received 26 October 2018; published 23 April 2019)

Background: The density-dependent symmetry energy coefficient plays a crucial role in understanding a variety of issues in nuclear physics as well as nuclear astrophysics. It is quite interesting and crucial to determine the symmetry energy coefficient and its related observables for neutron-rich thermally fissile nuclei at finite temperature.
Purpose: We evaluate the symmetry energy coefficient, neutron pressure, and symmetry energy curvature of a finite nucleus from the corresponding quantities of infinite nuclear matter. Moreover, we correlate an effective symmetry energy coefficient and its related observables with the neutron skin thickness of neutron-rich thermally fissile nuclei at a finite temperature.
Methods: The temperature-dependent relativistic mean field model (TRMF) is used to obtain the ground and excited state bulk properties of finite nuclei and the energy density, pressure, and the symmetry energy for infinite nuclear matter. The TRMF model with FSUGarnet, IOPB-I, and NL3 parameter sets is used for the present analysis. The effective nuclear matter properties are used to estimate the corresponding quantities of finite nuclei by using the local density approximation.
Results: Nuclear bulk properties such as binding energy, quadrupole deformation, root-mean-square charge radius of the nuclei, and the equation of state and symmetry energy for infinite symmetric nuclear matter are estimated within the TRMF model. The nuclear matter observables at the local density of the nuclei serve as an input to obtain the effective symmetry energy coefficient, neutron pressure, and the symmetry energy curvature of ^{234,236,250}U and ^{240}Pu nuclei. The influence of temperature and density on these properties for neutron-rich thermally fissile nuclei is observed. A correlation is established between the neutron skin thickness and the neutron pressure of the nuclei.
Conclusions: The studied properties of nuclei such as effective symmetry energy coefficient, neutron pressure and symmetry energy curvature can be used in the synthesis of neutron-rich thermally fissile nuclei. The method presented here (fully microscopic) can be used further to study the properties of exotic and superheavy nuclei from the corresponding quantities of nuclear matter and vice versa.

DOI: 10.1103/PhysRevC.99.044314

I. INTRODUCTION

Thermally fissile nuclei have the tendency to undergo fission even when a zero energy neutron (at room temperature) strikes them. In nature, ^{233,235}U and ^{239}Pu are thermally fissile. Of these, ^{235}U is naturally available with an isotopic fractional abundance of $\approx$0.7% [1]. ^{233}U and ^{239}Pu are formed by ^{232}Th and ^{238}U, respectively, through neutron absorption and subsequent β decays. It is well known that these nuclei have a great impact on society. One of the applications of thermally fissile nuclei is their use in controlled energy production. It is important to mention that Satpathy *et al.*, have found several neutron-rich uranium and thorium isotopes showing thermally fissile behavior [2]. These predicted neutron-rich thermally fissile nuclei can produce more energy than the naturally available thermally fissile nuclei. ^{250}U is one these. Due to the great importance of thermally fissile nuclei, it is worth studying their properties.

Several studies have been carried out to investigate structural properties and reaction dynamics of the thermally fissile nuclei and the isotopic series of actinide nuclei [3–7]. In our previous work [8], we studied the ground and excited state bulk properties of ^{234,236}U and ^{240}Pu nuclei. We have also investigated the properties (specifically, fission parameters) of the neutron-rich thermally fissile $^{244–262}$Th and $^{246–264}$U nuclei within the relativistic mean field model at finite temperature (T) [9]. Apart from the other bulk properties of a nucleus, it is also fruitful to know the properties, such as the symmetry energy coefficient, neutron pressure, and symmetry energy curvature, which can be helpful in synthesizing neutron-rich superheavy and exotic nuclei. In a fission process, the thermally fissile nuclei ^{233,235}U and ^{239}Pu absorb a slow neutron and make the compound nuclei ^{234,236}U and ^{240}Pu, respectively. These compound nuclei then fission into fragments and emit neutrons. Neutron-rich thermally fissile nuclei undergo

multifragment fission, an exotic decay mode in which, along with fragments, several prompt scission neutrons are emitted from the neck [2]. This fission process is directly connected with the neutron multiplicity of the surface region. It is thus of interest to know the temperature-dependent effective symmetry energy and its related observables for thermally fissile nuclei.

The nuclear symmetry energy plays a crucial role in different areas of nuclear physics, for example, in the structure of ground state nuclei [10–12], the dynamics of heavy-ion reactions [13,14], the physics of giant collective excitation [15], and the structure, dynamics, and composition of neutron stars [16,17]. It also determines various neutron star properties such as their cooling rates, crust thickness, mass-radius relationship, and moment of inertia [18]. Isospin asymmetry in nuclear matter arises due to differences in proton and neutron densities and masses. It is remarked in Ref. [19] that the density type isospin asymmetry is described by ρ meson (isovector-vector) exchange and the mass type asymmetry by δ meson (isovector-scalar) exchange. The symmetry energy is nearly equal to the energy cost used to convert symmetric nuclear matter to asymmetric matter. Astrophysical observations and the availability of exotic beams have increased interest in the symmetry energy. Furthermore, the internal configuration of a nuclear system (especially, of a neutron-rich nucleus) such as its distribution of nucleons, interaction strengths, and the nucleon dynamics influence the neutron pressure and the observables related to it.

Due to the importance of the symmetry energy, its characterization through experiment is a crucial step towards our capability of interpreting neutron-rich nuclei and neutron star matter. However, the symmetry energy is not a directly measurable quantity. It is extracted from the observables related to it. It has been found that the radius of a neutron star is correlated to the density dependence of the symmetry energy at the saturation point [20]. Theoretically, one observes that the slope parameter (L coefficient), and hence the pressure, is strongly correlated to the neutron skin thickness of ^{208}Pb [21–24] and the radius of a neutron star. Even the precise measurement of neutron skin thickness is difficult, yet it is a sensitive probe of the nuclear symmetry energy. Danielewicz has demonstrated that the ratio of the bulk symmetry energy to the surface symmetry energy is correlated to the neutron skin thickness [25]. The findings of Lee *et al.*, show that the surface symmetry energy term is more sensitive to temperature than the volume energy term [26]. Furthermore, the dependence of the symmetry energy on density and temperature have a crucial role in explaining various phenomena in heavy ion collisions, supernovae explosions, the liquid-gas phase transition of asymmetric nuclear matter, and mapping the location of the neutron drip line in the nuclear landscape [20,27,28].

The importance of the symmetry energy and its sensitivity to temperature and density have motivated us to study it in neutron-rich thermally fissile nuclei. In this paper, we study the symmetry energy, neutron pressure, and symmetry energy curvature of ^{234,236,250}U and ^{240}Pu at finite temperature. The motivation behind choosing these nuclei has already been stated, i.e., the thermally fissile nature of the nuclei and their importance for energy production. The symmetry energy of finite nuclei at saturation density has been studied by using various formulas of liquid drop models [29–32], the random phase approximation based on the Hartree-Fock (HF) approach [33], the energy density functional of the Skyrme force [34–37], the relativistic Lagrangian with density-dependent meson-nucleon vertex function [38], the relativistic nucleon-nucleon interaction [39,40], and a local density approximation [41–43]. In Refs. [44–47], the surface properties of nuclei have been studied by using the corresponding quantities of nuclear matter within the Brueckner energy density functional [48,49] into the coherent density fluctuation model (CDFM) [45,50]. Recently, Bhuyan *et al.* studied the effective surface properties, such as the symmetry energy, neutron pressure, and symmetry energy curvature of nuclei, by using the bulk properties from a relativistic mean field model as the inputs to the CDFM [51]. In our previous work, we found that the symmetry energy coefficient is sensitive to temperature as well as to the force parameters [8]. Within a Thomas-Fermi model, the density of a nucleus is calculated by subtracting the density profile of a gas phase from that of the liquid-gas phase [52–55]. This density (obtained through a subtraction procedure) is then used to calculate the rest of the properties of a nucleus. In the present analysis, we calculate the densities of the nuclei along with some of the ground and excited state properties within the temperature-dependent relativistic mean field (TRMF) model by considering particle number conservation. The properties of symmetric nuclear matter are also obtained within the TRMF formalism, which are further used to calculate the corresponding quantities of finite nuclei.

The paper is organized as follows: In Sec. II, we present the formalism followed to carry out the present analysis. We outline the TRMF and local density approximation models in this section. The numerical results and discussions are given in Sec. III. Finally, the work is summarized with a brief conclusion in Sec. IV.

II. FORMALISM

In this section, we outline the formalism followed to calculate the temperature-dependent symmetry energy and related quantities for nuclei. The calculations involve the following steps: (i) we estimate the nuclear matter observables and the ground and excited state bulk properties of the nuclei at finite temperature within the TRMF model; (ii) the temperature-dependent properties of symmetric nuclear matter at the local density of the nuclei are further used in a local density approximation to calculate the corresponding quantities of finite nuclei.

A. Temperature-dependent relativistic mean field (TRMF) model

Relativistic mean field (RMF) theory is the relativistic generalization of nonrelativistic Hartree or Hartree-Fock-Bogoliubov theory. In the RMF model, nucleons are assumed to interact with each other through the exchange of mesons. The advantage of using RMF over a nonrelativistic model is that it automatically takes the spin-orbit interaction into

consideration. Further, this model is capable of predicting the ground and excited state bulk properties of nuclei over the whole nuclear landscape. In principle, the mean field Lagrangian has an infinite number of terms with all possible types of self- and cross-couplings. To handle the RMF numerically, ratios of fields and nucleon masses are used in a truncation scheme as a constraint on naturalness. We have used the RMF Lagrangian having contributions of σ, ω, and ρ meson fields up to fourth order and for the rest of the mesons up to second order, which has been shown to be a good approximation for predicting finite nuclei and nuclear matter observables with good precision [56]. The energy density, obtained by solving the RMF Lagrangian and applying a mean field approximation, is given as

$$\begin{aligned}\mathcal{E}(r,T) = \sum_i n_i(T)\varphi_i^\dagger(r)\Big\{ & -i\boldsymbol{\alpha}\cdot\boldsymbol{\nabla} + \beta[M - \Phi(r) - \tau_3 D(r)] + W(r) + \frac{1}{2}\tau_3 R(r) + \frac{1+\tau_3}{2}A(r) \\ & - \frac{i\beta\boldsymbol{\alpha}}{2M}\cdot\left(f_\omega \boldsymbol{\nabla} W(r) + \frac{1}{2}f_\rho \tau_3 \boldsymbol{\nabla} R(r)\right)\Big\}\varphi_i(r) + \left(\frac{1}{2} + \frac{\kappa_3}{3!}\frac{\Phi(r)}{M} + \frac{\kappa_4}{4!}\frac{\Phi^2(r)}{M^2}\right)\frac{m_s^2}{g_s^2}\Phi^2(r) \\ & - \frac{\zeta_0}{4!}\frac{1}{g_\omega^2}W^4(r) + \frac{1}{2g_s^2}\left(1 + \alpha_1\frac{\Phi(r)}{M}\right)[\nabla\Phi(r)]^2 - \frac{1}{2g_\omega^2}\left(1 + \alpha_2\frac{\Phi(r)}{M}\right)[\nabla W(r)]^2 \\ & - \frac{1}{2}\left(1 + \eta_1\frac{\Phi(r)}{M} + \frac{\eta_2}{2}\frac{\Phi^2(r)}{M^2}\right)\frac{m_\omega^2}{g_\omega^2}W^2(r) - \frac{1}{2e^2}[\nabla A(r)]^2 - \frac{1}{2g_\rho^2}(\nabla R(r))^2 \\ & - \frac{1}{2}\left(1 + \eta_\rho\frac{\Phi(r)}{M}\right)\frac{m_\rho^2}{g_\rho^2}R^2(r) - \Lambda_\omega[R^2(r)\times W^2(r)] + \frac{1}{2g_\delta^2}[\nabla D(r)]^2 + \frac{1}{2}\frac{{m_\delta}^2}{g_\delta^2}[D^2(r)],\end{aligned} \tag{1}$$

where Φ, W, R, D, and A are the fields of the $\sigma, \omega, \rho, \delta$ mesons and photon, respectively, which are redefined as $\Phi = g_\sigma\sigma$, $W = g_\omega\omega^0$, $R = g_\rho\rho^0$, and $A = eA^0$. The constants $g_\sigma, g_\omega, g_\rho$, g_δ, $\frac{e^2}{4\pi}$ are the coupling strengths and $m_\sigma, m_\omega, m_\rho$, and m_δ are the masses for the $\sigma, \omega, \rho, \delta$ mesons and photon, respectively.

Temperature is introduced in the RMF formalism through the occupation factor n_i by using a Fermi-Dirac distribution function, where i stands for a nucleon state. The energy density of the Dirac fields and the nucleon densities are multiplied by the occupation factor. The temperature-dependent occupation factor is given as

$$\begin{aligned}n_i(T) = & \frac{1}{2}\left(1 - \frac{\epsilon_i - \lambda}{\tilde{\epsilon}_i}\right)[1 - f(\tilde{\epsilon}_i, T)] \\ & + \frac{1}{2}\left(1 + \frac{\epsilon_i - \lambda}{\tilde{\epsilon}_i}\right)f(\tilde{\epsilon}_i, T),\end{aligned} \tag{2}$$

with

$$\begin{aligned}f(\tilde{\epsilon}_i, T) &= \frac{1}{(1 + \exp[\tilde{\epsilon}_i/T])}, \\ \tilde{\epsilon}_i &= \sqrt{(\epsilon_i - \lambda)^2 + \triangle^2}.\end{aligned} \tag{3}$$

The function $f(\tilde{\epsilon}_i, T)$ represents the Fermi-Dirac distribution for quasiparticle energy $\tilde{\epsilon}_i$. λ and δ are the nucleon chemical potential and the pairing gap parameter. The detailed formalism of the temperature dependence of the RMF can be found in Refs. [8,57–60] and the description of the RMF Lagrangian, used in this work, can be found in Ref. [19].

B. Temperature-dependent equation of state and nuclear matter properties

Energy and pressure density. The temporal ($\langle T_{00}\rangle$) and spatial ($\langle T_{ii}\rangle$) components of the energy-momentum tensor $\langle T_{\mu\nu}\rangle$ give the energy density and pressure of the system [61]. For static uniform infinite nuclear matter, the derivatives of the meson field and electromagnetic interaction vanish. The expressions for energy density and pressure at finite temperature without pairing are given by [19,62,63]:

$$\begin{aligned}\mathcal{E}(T) = & \frac{2}{(2\pi)^3}\int d^3k\epsilon_i^*(k)(f_{i+} + f_{i-}) + \rho W \\ & + \frac{m_s^2\Phi^2}{g_s^2}\left(\frac{1}{2} + \frac{\kappa_3}{3!}\frac{\Phi}{M} + \frac{\kappa_4}{4!}\frac{\Phi^2}{M^2}\right) \\ & - \frac{1}{2}m_\omega^2\frac{W^2}{g_\omega^2}\left(1 + \eta_1\frac{\Phi}{M} + \frac{\eta_2}{2}\frac{\Phi^2}{M^2}\right) - \frac{1}{4!}\frac{\zeta_0 W^4}{g_\omega^2} \\ & + \frac{1}{2}\rho_3 R - \frac{1}{2}\left(1 + \frac{\eta_\rho\Phi}{M}\right)\frac{m_\rho^2}{g_\rho^2}R^2 \\ & - \Lambda_\omega(R^2\times W^2) + \frac{1}{2}\frac{m_\delta^2}{g_\delta^2}(D^2),\end{aligned} \tag{4}$$

$$\begin{aligned}P(T) = & \frac{2}{3(2\pi)^3}\int d^3k\frac{k^2}{\epsilon_i^*(k)}(f_{i+} + f_{i-}) \\ & - \frac{m_s^2\Phi^2}{g_s^2}\left(\frac{1}{2} + \frac{\kappa_3}{3!}\frac{\Phi}{M} + \frac{\kappa_4}{4!}\frac{\Phi^2}{M^2}\right) \\ & + \frac{1}{2}m_\omega^2\frac{W^2}{g_\omega^2}\left(1 + \eta_1\frac{\Phi}{M} + \frac{\eta_2}{2}\frac{\Phi^2}{M^2}\right) \\ & + \frac{1}{4!}\frac{\zeta_0 W^4}{g_\omega^2} + \frac{1}{2}\left(1 + \frac{\eta_\rho\Phi}{M}\right)\frac{m_\rho^2}{g_\rho^2}R^2 \\ & + \Lambda_\omega(R^2\times W^2) - \frac{1}{2}\frac{m_\delta^2}{g_\delta^2}(D^2),\end{aligned} \tag{5}$$

with the equilibrium distribution functions defined as

$$f_{i_\pm} = \frac{1}{1+\exp[(\epsilon_i^* \mp \nu_i)/T}, \tag{6}$$

where $\epsilon_i^* = (k^2 + M_i^{*2})^{1/2}$ $(i = p, n)$, $M_{p,n}^* = M_{p,n} - \Phi \mp D$, k is the momentum of nucleon, and the nucleon effective chemical potential is given by

$$\nu_i = \mu_i - W - \tfrac{1}{2}\tau_3 R, \tag{7}$$

where τ_3 is the third component of the isospin operator.

Symmetry energy and incompressibility coefficient. The binding energy per nucleon $\mathcal{E}/A = e(\rho, \alpha)$ (where ρ is the baryon density) can be expanded in a Taylor series in terms of the isospin asymmetry parameter α $(=\frac{\rho_n-\rho_p}{\rho_n+\rho_p})$:

$$e^{NM}(\rho,\alpha) = \frac{\mathcal{E}}{\rho_B} - M = e^{NM}(\rho, \alpha = 0) + S^{NM}(\rho)\alpha^2 + O^{NM}(\alpha^4), \tag{8}$$

where $e(\rho, \alpha = 0)$ is the energy density of symmetric nuclear matter (SNM) and $S(\rho)$ is the symmetry energy of the system, as defined below. Odd powers of α are forbidden by the isospin symmetry. The terms proportional to α^4 and higher order are found to be negligible, and

$$S^{NM}(\rho) = \frac{1}{2}\left[\frac{\partial^2 e^{NM}(\rho,\alpha)}{\partial\alpha^2}\right]_{\alpha=0}. \tag{9}$$

Near the saturation density ρ_0, the symmetry energy can be expanded in a Taylor series as

$$S^{NM}(\rho) = J^{NM} + L^{NM}\mathcal{Y} + \tfrac{1}{2}K_{\rm sym}^{NM}\mathcal{Y}^2 + \tfrac{1}{6}Q_{\rm sym}^{NM}\mathcal{Y}^3 + O^{NM}[\mathcal{Y}^4], \tag{10}$$

where $J^{NM} = S^{NM}(\rho_0)$ is the symmetry energy at saturation and $\mathcal{Y} = \frac{\rho-\rho_0}{3\rho_0}$. The coefficients $L^{NM}(\rho_0)$, $K_{\rm sym}^{NM}(\rho_0)$, and $Q_{\rm sym}^{NM}$ are defined as

$$L^{NM} = 3\rho\frac{\partial S^{NM}(\rho)}{\partial\rho}\bigg|_{\rho=\rho_0} = \frac{3P^{NM}}{\rho}\bigg|_{\rho=\rho_0}, \tag{11}$$

$$K_{\rm sym}^{NM} = 9\rho^2\frac{\partial^2 S^{NM}(\rho)}{\partial\rho^2}\bigg|_{\rho=\rho_0}, \tag{12}$$

$$Q_{\rm sym}^{NM} = 27\rho^3\frac{\partial^3 S^{NM}(\rho)}{\partial\rho^3}\bigg|_{\rho=\rho_0}. \tag{13}$$

Here, L^{NM}, P^{NM}, and $K_{\rm sym}^{NM}$ represent the slope parameter of the symmetry energy, the neutron pressure, and the symmetry energy curvature at the saturation density, respectively. In this work, the properties of symmetric nuclear matter are temperature dependent. Those will be used to calculate the corresponding quantities of the nuclei in the local density approximation.

C. Local density approximation (LDA)

The effective bulk properties of a nucleus can be found by using the LDA once its density profile is known. In the LDA, the symmetry energy coefficient $S(T)$ can be defined as [41–43]

$$S(T)\left(\frac{N-Z}{A}\right)^2 = \frac{1}{A}\int \rho(r)S^{NM}[\rho(r), T]\alpha^2(r)d\mathbf{r}, \tag{14}$$

where $S^{NM}[\rho(r), T]$ is the symmetry energy coefficient of infinite symmetric nuclear matter at finite temperature (T) and at the local density $\rho(r)$ of a nucleus, and $\alpha(r)$ is the isospin asymmetry parameter defined earlier. Expressions similar to those in Eq. (14) can be used to find the neutron pressure and symmetry energy curvature by replacing $S^{NM}[\rho(r), T]$ with the corresponding nuclear matter quantities at the local density of a nucleus. $S^{NM}[\rho(r), T]$ is found from Eq. (10), where ρ is the density of a nucleus $\rho(r)$. Similarly, $P^{NM}[\rho(r), T]$ and $K^{NM}[\rho(r), T]$ at the density of a nucleus are found by using Eqs. (11) and (12), respectively. As stated earlier, the density distribution for a nucleus is calculated within the TRMF model (Hartree approximation) for a given parameter set, with the equations of motion being solved self-consistently [8,56]. As a result, the density from the Hartree approximation is purely quantal one with a well-defined surface. There are thus no corrections to be included externally for the surface, as would be the case for a semiclassical model [64–69]. Generally, semiclassical methods such as the extended Thomas-Fermi (ETF) method [67] and the relativistic extended Thomas-Fermi (RETF) formalism [64] are based on the Wigner-Kirkwood (WK) $\hbar$ expansion of the density matrix [65,66] of a nucleus. In this case, the calculated density of a nucleus does not have a well-defined surface, which is the expected error (qualitative) in assuming the LDA for the symmetry energy of a finite nucleus. To sort out the deficiencies of the Thomas-Fermi approximations, and thus to provide a more accurate description of the nuclear surface, at least $\hbar^2$-order gradient corrections coming from inhomogeneity and nonlocal effects have to be included in the energy density functional [64]. It is worth mentioning that the density obtained here from Hartree approximation can be directly used in Eq. (14) for further calculations [8,41,56,69] without adding surface corrections externally.

In general, the symmetry energy coefficient of a finite nucleus is a bulk property that mainly depends on the isospin asymmetry of the nucleus. The symmetry energy of a nucleus can be written in terms of volume and surface symmetry energy coefficients in order to study its approximate mass dependence (see Eq. (2) of Ref. [41]). The surface term is important in determining the symmetry energy of light mass nuclei and it becomes small for heavy and superheavy nuclei, since the surface symmetry energy coefficient is proportional to $A^{-1/3}$, where A is the mass number [32,41]. The volume symmetry energy is almost independent of the shape degrees of freedom of a nucleus [32]. In [37], one can find that the relative change in the symmetry energy with very large deformation ($\beta_2 \approx 0.6$) is around 0.4 MeV. It is also mentioned in Ref. [37] that the effect of deformation on the symmetry energy decreases with respect to the mass number. Here we study the uranium and plutonium isotopes, which are superheavy in nature, with ground state deformations of magnitude $\beta_2 \approx 0.2$. Hence the effects of deformation on the symmetry energy are very small and, for the sake of

TABLE I. The parameter sets NL3 [72], FSUGarnet [71], and IOPB-I [19] are listed. The nucleon mass M is 939.0 MeV. All the coupling constants are dimensionless, except k_3 which is in fm^{-1}.

	NL3	FSUGarnet	IOPB-I
m_s/M	0.541	0.529	0.533
m_ω/M	0.833	0.833	0.833
m_ρ/M	0.812	0.812	0.812
m_δ/M	0.0	0.0	0.0
$g_s/4\pi$	0.813	0.837	0.827
$g_\omega/4\pi$	1.024	1.091	1.062
$g_\rho/4\pi$	0.712	1.105	0.885
$g_\delta/4\pi$	0.0	0.0	0.0
k_3	1.465	1.368	1.496
k_4	−5.688	−1.397	−2.932
ζ_0	0.0	4.410	3.103
η_1	0.0	0.0	0.0
η_2	0.0	0.0	0.0
η_ρ	0.0	0.0	0.0
Λ_ω	0.0	0.043	0.024
α_1	0.0	0.0	0.0
α_2	0.0	0.0	0.0
$f_\omega/4$	0.0	0.0	0.0
$f_\rho/4$	0.0	0.0	0.0
β_σ	0.0	0.0	0.0
β_ω	0.0	0.0	0.0

computational simplicity, we have taken the monopole term (spherical equivalent) of the density distribution without changing the volume of a nucleus in the present analysis. The multipole decomposition of the density in terms of even values of the multipole index λ [70] is given as

$$\rho(r_\perp, z) = \sum_\lambda \rho_\lambda(r) P_\lambda(\cos\theta), \tag{15}$$

where P_λ is a Legendre polynomial and r is the radial variable.

III. RESULTS AND DISCUSSIONS

The main aim of this work is to study the symmetry energy coefficient S, neutron pressure P, and symmetry energy curvature $K_{\rm sym}$ of neutron-rich thermally fissile nuclei at finite temperature. In this work, we have taken ^{250}U as a representative case of the neutron-rich thermally fissile nuclei [2]. ^{234,236}U and ^{240}Pu are also studied because of the importance of the fission of the known thermally fissile ^{233,235}U and ^{239}Pu nuclei. Before proceeding to the observables described above, we have calculated ground and excited state properties of these nuclei. For the calculations, we have used the FSUGarnet [71], IOPB-I [19], and NL3 [72] parameter sets within the TRMF model. Among these, the NL3 [72] set is one of the best-known and most used RMF parameter sets and describes the properties of nuclei remarkably well over the nuclear chart. The FSUGarnet [71] and IOPB-I [19] are more recent parameter sets with the advantage that their equations of state are softer than that of the NL3 parameter set. In Table I, we have given the values of the parameters in these sets. In the relativistic mean field model, the field equations are solved self-consistently by taking an initial estimate of the deformation β_0 [19,51,71,72]. The mesonic and fermionic fields are expanded in terms of the deformed harmonic oscillator basis. The number of major shells for the fermionic and bosonic fields (NOF and NOB, respectively) have been taken as 14 and 20. At these values of NOF and NOB, we obtain a converged solution in this mass region.

A. Ground and excited state properties of the nuclei

The binding energy per particle (B/A), charge radius (R_c), and deformation parameter (β_2) of the nuclei ^{208}Pb, ^{234,236,250}U, and ^{240}Pu at finite temperature (T) with the FSUGarnet [71], IOPB-I [19], and NL3 [72] parameter sets are shown in Table III with the available experimental data [73,74]. The calculated values corresponding to all parameter sets are in good agreement with each other. These results are comparable to the corresponding experimental data at $T = 0$ MeV. All of the calculations show good agreement with the binding energy but slightly underestimate the deformation at $T = 0$. The IOPB-I parameter set furnishes changes in the radii that are slightly longer than those of the other sets at all values of the temperature. The binding energies obtained with the NL3 parameter set are slightly smaller than those of the other sets for $T > 0$. The binding energy and quadrupole deformation of the nuclei decrease with T. The temperature at which the deformation of a nucleus becomes zero is known as the critical temperature (T_c). For the IOPB-I set, the T_c value is obtained at a lower temperature than for the other sets.

B. Temperature-dependent symmetry energy of nuclear matter

In order to study the surface properties of the nuclei at finite T, we will use the corresponding temperature-dependent quantities of nuclear matter at the local density of the nuclei in the LDA. First, we reproduce the equations of state of symmetric nuclear matter (SNM) and pure neutron matter (PNM) at zero temperature, as have been presented in Ref. [19]. The energy density and pressure of SNM and PNM for the FSUGarnet (maroon dashed curve), IOPB-I (red dot-dashed curve), and NL3 (green solid curve) parameters sets are shown in Fig. 1. The upper-left panel of the figure represents the energy density of symmetric nuclear matter (SNM). It is clear from this panel of the figure that the FSUGarnet and IOPB-I EOSs are softer than that of NL3 set. FSUGarnet is the softest among the chosen parameter sets. The similar nature of the EOS of PNM is shown in the lower left panel. The shaded region is the range for the EOS obtained by Hebeler *et al.*, [75]. It can be seen in the figure (Fig. 1) that the energy densities corresponding to NL3 and FSUGarnet (it is even softer) do not pass through the low density region of pure neutron matter. Here, the EOS of IOPB-I passes comparatively close to the low as well as the high density region of the experimental band and through it in the intermediate region of the density, while that of FSUGarnet passes only through the high density region. The black curve (in the left panels) represents the DBHF data [76].

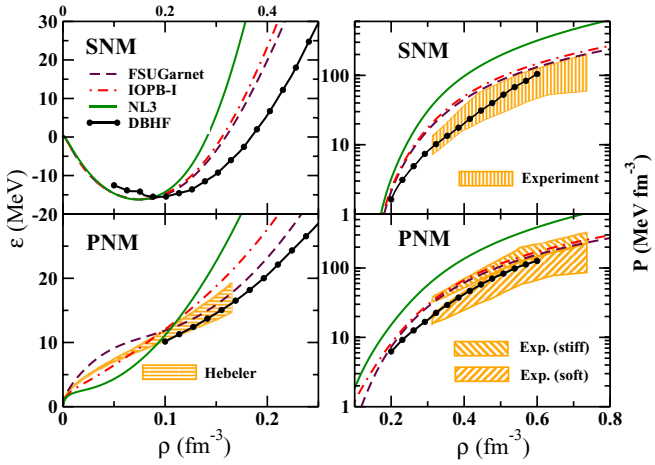

FIG. 1. The energy density and pressure for SNM and PNM at zero temperature with FSUGarnet, IOPB-I, and NL3 parameter sets. The calculated results are compared with the results by Hebeler [75], the DBHF equation of state [76,77], and the available experimental data [78].

The right panel of the figure shows the pressure of SNM (upper right) and PNM (lower right) for the same parameter sets. The black curve represents the BHF results of Baldo *et al.*, [77] and the shaded region is the experimentally consistent range of values [78]. In the case of SNM, both the FSUGarnet and IOPB-I sets satisfy the experimental limits, while for PNM they only pass through the upper boundary of the experimental soft EOS. In the cases of both SNM and PNM, NL3 is far from the experimental bounds. The softer nature of the EOSs of FSUGarnet and IOPB-I is attributed to the cross coupling of ω and ρ mesons [19]. This is one of the reasons for choosing these parameter sets in this work. The values of SNM properties such as the energy density ($\mathcal{E}$), symmetry energy J^{NM}, symmetry energy curvature ($K_{\rm sym}^{NM}$), slope parameter of the symmetry energy (L^{NM}), and $Q_{\rm sym}^{NM}$ at the saturation density ρ_0 are given in Table II.

The symmetry energy of SNM is shown in Fig. 2. The left panel of the figure represents the symmetry energy for the FSUGarnet (maroon dashed curve), IOPB-I (red dot-dashed curve), and NL3 (green solid curve) parameter sets at $T = 0$. The parameter sets produce different symmetry energy curves, clearly visible in the figure. We show the symmetry

TABLE II. The nuclear matter properties at saturation density ρ_0(fm^{-3}) for the three parameter sets.

	NL3	FSUGarnet	IOPB-I
ρ_0 (fm^{-3})	0.148	0.153	0.149
$\mathcal{E}_0$ (MeV)	−16.29	−16.23	−16.10
M^*/M	0.595	0.578	0.593
J^{NM} (MeV)	37.43	30.95	33.30
L^{NM} (MeV)	118.65	51.04	63.58
$K_{\rm sym}^{NM}$ (MeV)	101.34	59.36	−37.09
$Q_{\rm sym}^{NM}$ (MeV)	177.90	130.93	862.70

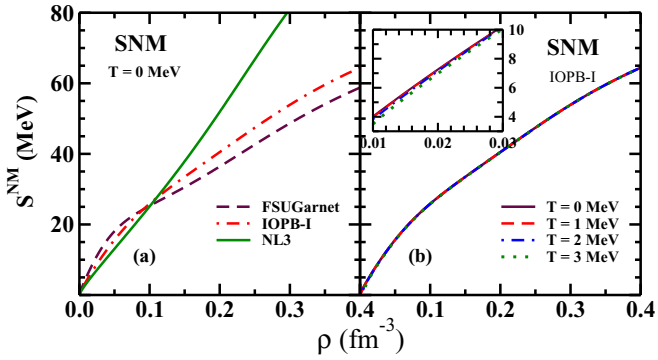

FIG. 2. (a) The symmetry energy (S^{NM}) of infinite SNM at zero temperature for the FSUGarnet, IOPB-I, and NL3 parameter sets. (b) The same quantity at finite temperature corresponding to IOPB-I. The zoomed part shows S^{NM} at low density.

energy of SNM at finite T for the IOPB-I parameter set as a representative case in the right panel of Fig. 2. The effects of temperature on nuclear matter can be observed at higher values of T. Here, we have calculated the symmetry energy for $T = 0$, 1, 2, and 3 MeV. The symmetry energy S^{NM} at these temperatures is almost the same. The minute difference at low density can be seen in the zoomed part of the figure. This minute difference causes a significant change in the value of $S(T)$ of a nucleus at finite T. The quantities involved in the expansion of the symmetry energy at the local density of a nucleus [Eq. (10)] are J^{NM}, L^{NM}, and $K_{\rm sym}^{NM}$ at the saturation point of nuclear matter. These quantities are not considered as constant values throughout the calculation of the temperature-dependent symmetry energy. Rather, they slightly change due to the temperature. Thus, in the calculation of the symmetry energy of nuclear matter at the local density of a nucleus, we have taken the temperature-dependent saturation point to get numerically consistent results. Similarly, all the quantities at the saturation point in Eq. (10) are evaluated at finite T.

C. Nuclear density and symmetry energy at the local nuclear density

The spherical equivalent densities of the deformed nuclei ^{234,250}U at finite T obtained within the TRMF model with the IOPB-I parameter set as a representative case are shown in Fig. 3. A color key is in the left panel. The effect of T on the densities can be observed from the figure. At finite temperature, the random motion of the nucleons is increased. As a result, their density distribution is changed. The central density of the nuclei is found to decrease with the increase of T. Consequently, the nucleons are pushed towards the surface and hence the surface density of nuclei has a slight enhancement with T. The effect of temperature on the size of a nucleus can also be observed from Table III, where it is found to be growing. The zoomed part of the figure shows the surface part of the density. The calculated densities are used to obtain the effective surface properties of the nuclei through Eq. (14).

The symmetry energy of nuclear matter at the local density of ^{250}U as a representative case is shown in Fig. 4. The left panel of the figure exhibits the symmetry energy at zero

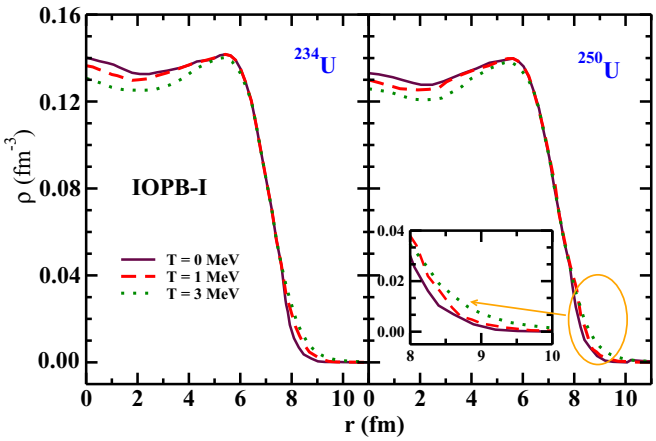

FIG. 3. The densities of the nuclei ^{234}U (left panel) and ^{250}U (right panel) corresponding to the IOPB-I set at finite T. The zoomed part shows the effect of T on the density at the surface of the nuclei.

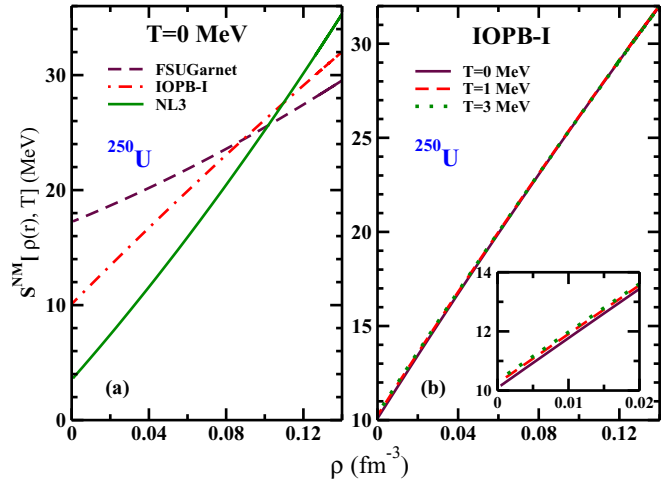

FIG. 4. The symmetry energy of nuclear matter $S^{NM}[\rho(r), T]$ at the local density of ^{250}U (a) at $T = 0$ MeV corresponding to the FSUGarnet, IOPB-I, and NL3 parameter sets, and (b) at finite T corresponding to the IOPB-I set. The zoomed part of panel (b) shows the effect of T at low density.

temperature with the three parameter sets, while the right panel shows the same at finite T corresponding to the IOPB-I set. It is clear from the figure that the symmetry energy is very sensitive to the choice of the parameter set. The symmetry energy corresponding to FSUGarnet is larger while that corresponding to NL3 is smaller. This trend is reversed at higher values of the density, i.e., $\approx$0.10 fm^{-3}. The symmetry energy has a weak temperature dependence in the range of T considered. The zoomed part of the right panel shows this small effect of T at low nuclear density. This dependence is similar to that shown in Fig. 2.

D. The symmetry energy, neutron pressure, and symmetry energy curvature of finite nuclei

Figure 5 shows the temperature-dependent effective symmetry energy coefficient S of the nuclei ^{234,236,250}U and ^{240}Pu for the FSUGarnet (maroon dashed curve), IOPB-I (red dot-dashed curve), and NL3 (green solid curve) parameter sets. The values of S in all the cases decreases monotonically with T. The results corresponding to the IOPB-I set are intermediate to those corresponding to FSUGarnet and NL3. As mentioned above, the FSUGarnet set is the softest among the chosen sets while NL3 is the stiffest (see Fig. 1). Thus, the properties of the nuclei and nuclear matter predicted by IOPB-I lie in between those predicted by FSUGarnet and NL3 [8,19]. In the case of ^{236,250}U, the symmetry energy curve corresponding to IOPB-I is almost equal to that of FSUGarnet. Among the four nuclei, the $S(T)$ coefficient for ^{250}U is the smallest due to its large isospin asymmetry. A lower value of the symmetry energy enhances the rate of conversion of protons to neutrons through electron capture [16,79]. The low value of $S(T)$ for ^{250}U means that the conversion of

TABLE III. The calculated binding energy per particle (B/A) (MeV), charge radius (R_c) (fm) and deformation parameter β_2 of the nuclei ^{234,236,250}U and ^{240}Pu at finite temperature T (MeV) are tabulated and compared with the available experimental data [73,74].

Temperature	^{234}U			^{236}U			^{240}Pu			^{250}U			Parameter
	B/A	R_c	β_2	B/A	R_c	β_2	B/A	R_c	β_2	B/A	R_c	β_2	
$T = 0$	7.60	5.84	0.20	7.57	5.86	0.22	7.56	5.91	0.24	7.41	5.95	0.22	FSUGar.
	7.61	5.88	0.20	7.59	5.90	0.22	7.57	5.95	0.25	7.43	5.99	0.23	IOPB-I
	7.60	5.84	0.24	7.58	5.86	0.25	7.55	5.90	0.27	7.42	5.94	0.22	NL3
	7.60	5.83	0.27	7.59	5.84	0.27	7.56	5.87	0.29				Exp.
$T = 1$	7.55	5.83	0.16	7.54	5.85	0.19	7.51	5.90	0.23	7.37	5.94	0.20	FSUGar.
	7.56	5.85	0.02	7.55	5.89	0.20	7.52	5.94	0.23	7.39	5.99	0.22	IOPB-I
	7.51	5.84	0.22	7.50	5.85	0.24	7.47	5.90	0.25	7.33	5.94	0.21	NL3
$T = 2$	7.35	5.82	0.02	7.32	5.83	0.02	7.29	5.87	0.04	7.15	5.92	0.05	FSUGar.
	7.35	5.86	0.01	7.33	5.88	0.02	7.29	5.91	0.03	7.16	5.96	0.03	IOPB-I
	7.28	5.81	0.00	7.26	5.82	0.00	7.22	5.86	0.00	7.09	5.91	0.00	NL3
$T = 3$	6.95	5.86	0.02	6.94	5.87	0.02	6.90	5.90	0.02	6.75	5.95	0.02	FSUGar.
	6.94	5.90	0.01	6.93	5.91	0.02	6.89	5.95	0.02	6.75	6.00	0.01	IOPB-I
	6.87	5.84	0.00	6.85	5.86	0.00	6.82	5.91	0.00	6.68	5.94	0.00	NL3

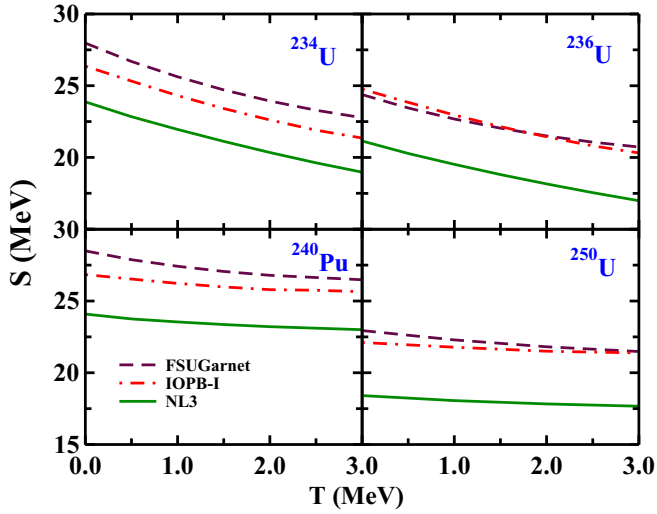

FIG. 5. The effective symmetry energy coefficient (S) of ^{234,236,250}U and ^{240}Pu at finite T.

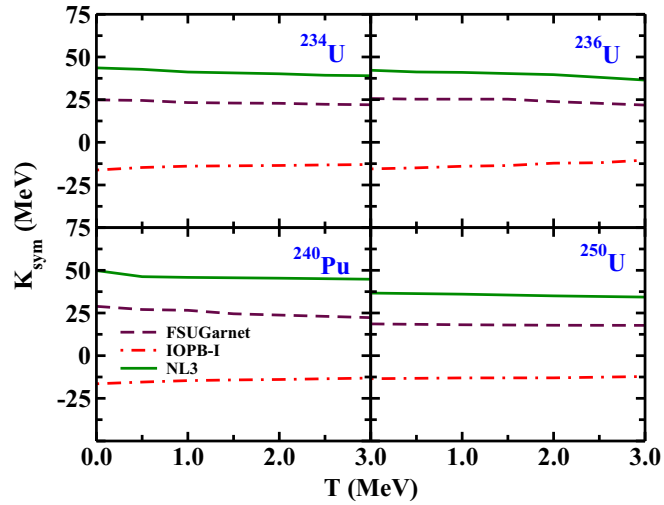

FIG. 7. The symmetry energy curvature ($K_{\rm sym}$) of the nuclei ^{234,236,250}U and ^{240}Pu at finite T.

asymmetric to symmetric matter requires a smaller amount of energy. Similarly, the lowering of the values of symmetry energy coefficient at higher T imply that less energy is needed to convert a neutron to proton or vice versa. It can be remarked here that the rate of β decay will increase with T (i.e., in the excited state of a nucleus).

The effects of T on the effective neutron pressure and symmetry energy curvature are shown in Figs. 6 and 7, respectively. The trend of the curves of P and $K_{\rm sym}$ is similar to that observed in the case of S. But, the order of the curves corresponding to the parameter sets is different. Here, FSUGarnet predicts smaller values of the pressure compared to the IOPB-I and NL3 sets. It implies that the softer the EOS, the smaller the pressure of the system is. The ^{250}U nucleus has smaller P and $K_{\rm sym}$ values than the other nuclei. This behavior can also be attributed to the large isospin asymmetry of the

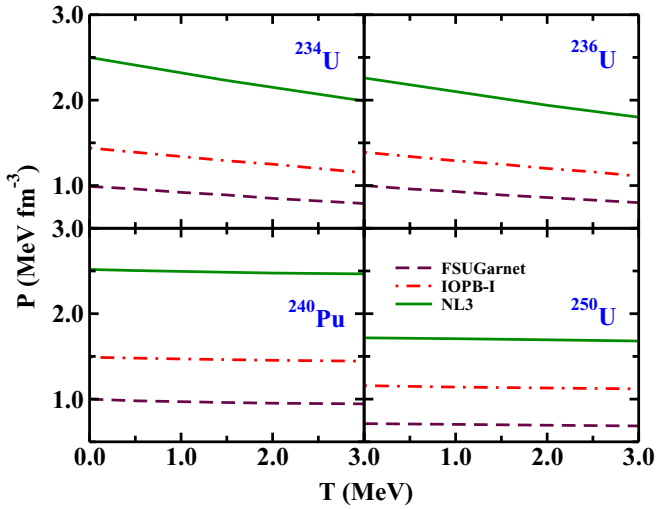

FIG. 6. The effective neutron pressure (P) of the nuclei ^{234,236,250}U and ^{240}Pu at finite T for the chosen parameter sets.

nucleus. The neutron pressure decreases with T because the volume of a nucleus expands (i.e., the radius increases as seen in Table III) as T increases. The rate of emission of neutrons from a nucleus also increases with T [80], which leads to decrease in the pressure. The values of $K_{\rm sym}$ corresponding to the IOPB-I set are negative, which is consistent with the negative value of the symmetry energy curvature at the saturation density of nuclear matter (see Table II).

The skin thickness has been shown to be correlated with the effective surface properties in Refs. [44–47,51] over particular isotopic chains. It depends linearly on the surface properties of a nucleus with a kink at a magic/semimagic nucleus of an isotopic chain [44–47,51]. Although we have not considered a whole isotopic chain of nuclei, we have found a correlation among the skin thickness, symmetry energy, and the neutron pressure due to the variation in these quantities at finite T. Figure 8 shows the correlation between the effective symmetry energy coefficient and the skin thickness of the nuclei at finite T. The skin thickness of the nuclei grows with the temperature [8]. We have seen in Fig. 5 that the symmetry energy coefficient decreases with T. This implies that the symmetry energy coefficient should decrease with the increase of skin thickness at finite T. The same tendency is observed in Fig. 8. It is clear from the figure that NL3 predicts a larger neutron skin thickness, with lower values of symmetry energy coefficient compared to the other parameter sets. This decrease is monotonic in nature. In going to heavier nuclei, the curves become flatter, which means that slight changes in the symmetry energy coefficient lead to large changes in the skin thickness and vice verse.

The slope parameter (L coefficient), and thus the pressure [see Eq. (11)] have been shown to be strongly correlated with the neutron skin thickness of ^{208}Pb [21–24] and the radius of a neutron star. This motivates us to examine the correlation between the pressure of the finite nuclei and their neutron skin thickness. In Fig. 9, we show a linear correlation between the neutron pressure and the skin thickness of finite nuclei at $T = 0$ MeV for all four nuclei. The panels (a), (b), (c),

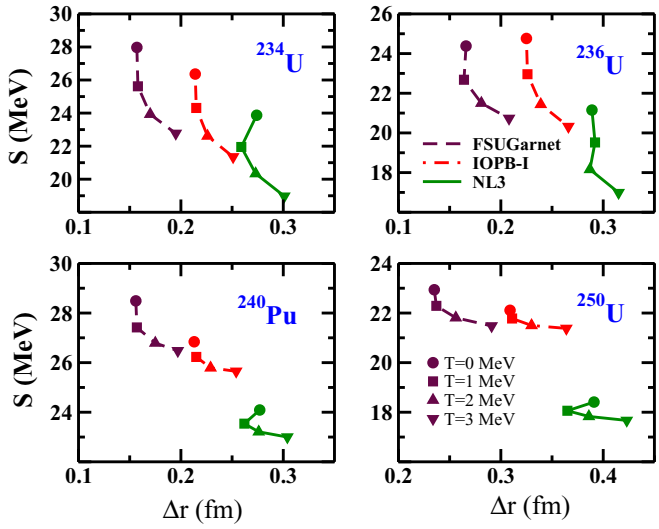

FIG. 8. The variation of the symmetry energy coefficient with the neutron skin thickness for the FSUGarnet, IOPB-I, and NL3 parameter sets. The circle, square, triangle up, and triangle down symbols correspond to the values at temperature 0, 1, 2, and 3 MeV.

and (d) of the figure contain the data of P versus Δr for the nuclei ^{234,236}U, ^{240}Pu and ^{250}U, respectively, with FSUGarnet, IOPB-I, and NL3 parameter sets. The skin thickness of the nuclei is increased with the parameter sets (going from softer to stiffer). One observes in Fig. 1 that the stiffer the EOS, the larger the pressure is for nuclear matter. A similar trend is obtained for finite nuclei. The neutron pressure is greater for the NL3 set, while it is a minimum for the parameter set FSUGarnet. Here, by fixing the temperature, the effects on pressure may be studied going from one force parameter to the others. The lines in the graph are the linear fitted curves (as $y = ax + b$) with the values of a and b (31.715, −2.523), (23.429, −1.644), (31.421, −2.399), and (19.177, −2.484)

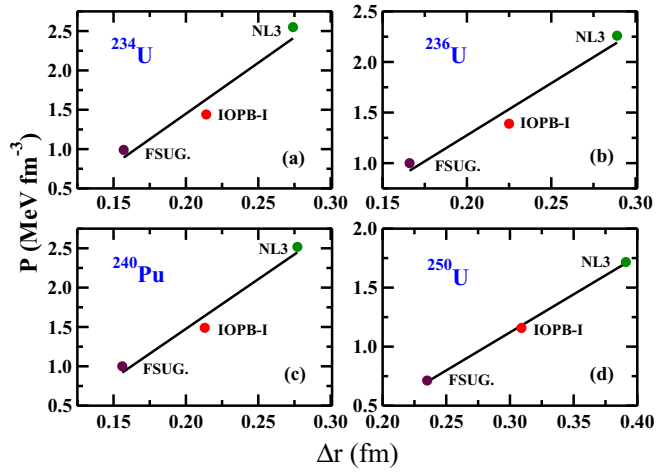

FIG. 9. The effective neutron pressure P for (a) ^{234}U, (b) ^{236}U, (c) ^{240}Pu, and (d) ^{250}U, as a function of the neutron skin thickness Δr for the three parameter sets FSUGarnet, IOPB-I, and NL3. The lines in all panels represent a linear fit.

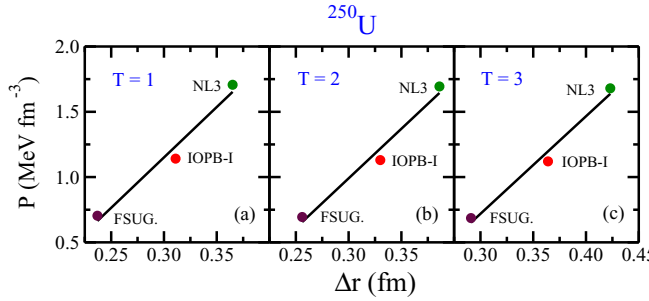

FIG. 10. The effective neutron pressure P as a function of the neutron skin thickness Δr for ^{250}U at temperatures $T = 1, 2, 3$ MeV [panels (a), (b), and (c), respectively] for the three parameter sets FSUGarnet, IOPB-I, and NL3. The lines in all panels represent a linear fit.

for ^{234,236}U, ^{240}Pu, and ^{250}U, respectively. This correlation is also seen when the temperature of the nuclei is increased (see Fig. 10).

IV. SUMMARY AND CONCLUSIONS

We have studied the effective bulk symmetry energy properties of ^{234,236,250}U and ^{240}Pu nuclei within the TRMF model. We have calculated the densities of the nuclei along with ground and excited state bulk properties at finite T within the axially deformed TRMF model. The nuclear matter EOS for SNM and PNM along with the symmetry energy and its related observables are also estimated within the TRMF formalism. We have used recently determined force parameter sets, i.e., FSUGarnet and IOPB-I, and compared the results with the widely accepted NL3 interaction. The nuclear matter properties are calculated at the local densities of the nuclei, which are further used in the LDA to calculate the corresponding properties of the nuclei. We have observed a minute effect of the temperature on the nuclear matter symmetry energy, which causes a significant change in the symmetry energy and related quantities of a nucleus according to its density profile. However, the effect of temperature on the calculated properties is almost the same irrespective of the parameter sets. The symmetry energy, neutron pressure, and symmetry energy curvature decrease with the increase of T, while the skin thickness increases. These properties are found to be smaller for ^{250}U due to its large isospin asymmetry, which enhances the rate of electron capture. The correlation among the calculated properties of the nuclei is found at finite T for each parameter set. The symmetry energy coefficient is found to vary inversely with the pressure. It is found that the softer the EOS is, the larger the symmetry energy coefficient and the smaller the neutron pressure of the nuclei are. The neutron pressure is linearly correlated with Δr at finite T, as calculated with all three parameter sets.

ACKNOWLEDGMENTS

We would like to thank Bharat Kumar, J. N. De, and B. K. Agrawal for fruitful discussions. A.Q. is grateful to IOPB for their hospitality and providing necessary computer

and library facilities required to carry out the work. Partial support from DST in the form of a fellowship for A.Q. is greatly acknowledged. M.B. and B.V.C. are grateful for the support by FAPESP Projects No. 2014/26195-5 and No. 2017/05660-0, by INCT-FNA Project No. 464898/2014-5, and by the CNPq - Brasil.

[1] National Nuclear Data Center, www.nndc.bnl.gov.
[2] L. Satpathy, S. K. Patra, and R. K. Choudhury, Pramana J. Phys. **70**, 87 (2008).
[3] B. Kumar, S. K. Biswal, S. K. Singh, and S. K. Patra, Phys. Rev. C **92**, 054314 (2015).
[4] M. T. Senthil Kannan, B. Kumar, M. Balasubramaniam, B. K. Agrawal, and S. K. Patra, Phys. Rev. C **95**, 064613 (2017).
[5] B. Kumar, M. T. Kannan, M. Balasubramaniam, B. K. Agrawal, and S. K. Patra, Phys. Rev. C **96**, 034623 (2017).
[6] J. E. Lynn, P. Talou, and O. Bouland, Phys. Rev. C **97**, 064601 (2018).
[7] S. Wuenschel, K. Hagel, M. Barbui, J. Gauthier, X. G. Cao, R. Wada, E. J. Kim, Z. Majka, R. Płaneta, Z. Sosin, A. Wieloch, K. Zelga, S. Kowalski, K. Schmidt, C. Ma, G. Zhang, and J. B. Natowitz, Phys. Rev. C **97**, 064602 (2018).
[8] A. Quddus, K. C. Naik, and S. K. Patra, J. Phys. G: Nucl. Part. Phys. **45**, 075102 (2018).
[9] A. Quddus, K. C. Naik, R. N. Panda, and S. K. Patra (unpublished).
[10] T. Niksić, D. Vretenar, and P. Ring, Phys. Rev. C **78**, 034318 (2008).
[11] N. Van Giai, B. V. Carlson, Z. Ma, and H. Wolter, J. Phys. G **37**, 064043 (2010).
[12] E. N. E. van Dalen and H. Müther, Int. J. Mod. Phys. **19**, 2077 (2010).
[13] B.-A. Li, L.-W. Chen, and C. M. Ko, Phys. Rep. **464**, 113 (2008).
[14] M. Colonna, J. Phys.: Conf. Ser. **168**, 012006 (2009).
[15] V. Rodin, Prog. Part. Nucl. Phys. **59**, 268 (2007).
[16] A. W. Steiner, M. Prakash, J. M. Lattimer, and P. J. Ellis, Phys. Rep. **411**, 325 (2005).
[17] J. M. Lattimer and M. Prakash, Phys. Rep. **621**, 127 (2016).
[18] *Nuclear Astrophysics*, in The 2015 Long Range Plan for Nuclear Science, https://science.energy.gov/∼/media/np/nsac/pdf/2015LRP/2015_LRPNS_091815.pdf (USDOE, 2015), p. 53.
[19] B. Kumar, S. K. Patra, and B. K. Agrawal, Phys. Rev. C **97**, 045806 (2018).
[20] J. M. Lattimer and M. Prakash, Phys. Rep. **442**, 109 (2007).
[21] B. A. Brown, Phys. Rev. Lett. **85**, 5296 (2000).
[22] R. J. Furnstahl, Nucl. Phys. A **706**, 85 (2002).
[23] M. Centelles, X. Roca-Maza, X. Viñas, and M. Warda, Phys. Rev. Lett. **102**, 122502 (2009).
[24] X. Roca-Maza, M. Centelles, X. Viñas, and M. Warda, Phys. Rev. Lett. **106**, 252501 (2011).
[25] P. Danielewicz, Nucl. Phys. A **727**, 233 (2003).
[26] S. J. Lee and A. Z. Mekjian, Phys. Rev. C **82**, 064319 (2010).
[27] V. Baran, M. Colonna, V. Greco, and M. Di Toro, Phys. Rep. **410**, 335 (2005).
[28] E. Baron, J. Cooperstein, and S. Kahana, Phys. Rev. Lett. **55**, 126 (1985).
[29] W. D. Myers and W. J. Swiatecki, Nucl. Phys. A **81**, 1 (1966).
[30] P. Möller, J. R. Nix, W. D. Myers, and W. J. Swiatecki, At. Data Nucl. Data Tables **59**, 185 (1995).
[31] K. Pomorski and J. Dudek, Phys. Rev. C **67**, 044316 (2003).
[32] N. Nikolov, N. Schunck, W. Nazarewicz, M. Bender, and J. Pei, Phys. Rev. C **83**, 034305 (2011).
[33] A. Carbone, G. Coló, A. Bracco, L.-G. Cao, P. F. Bortignon, F. Camera, and O. Wieland, Phys. Rev. C **81**, 041301(R) (2010).
[34] L.-W. Chen, C. M. Ko, and B.-A. Li, Phys. Rev. C **72**, 064309 (2005).
[35] S. Yoshida and H. Sagawa, Phys. Rev. C **73**, 044320 (2006).
[36] L.-W. Chen, C. M. Ko, B.-A. Li, and J. Xu, Phys. Rev. C **82**, 024321 (2010).
[37] M. Q. Hong, L. Min, C. L. Chun, and W. Ning, Sci. China-Phys. Mech. Astron. **58**, 082001 (2015).
[38] D. Vretenar, T. Niksic, and P. Ring, Phys. Rev. C **68**, 024310 (2003).
[39] C.-H. Lee, T. T. S. Kuo, G. Q. Li, and G. E. Brown, Phys. Rev. C **57**, 3488 (1998).
[40] B. K. Agrawal, Phys. Rev. C **81**, 034323 (2010).
[41] B. K. Agrawal, J. N. De, and S. K. Samaddar, Phys. Rev. Lett. **109**, 262501 (2012).
[42] S. K. Samaddar, J. N. De, X. Viñas, and M. Centelles, Phys. Rev. C **76**, 041602(R) (2007).
[43] J. N. De and S. K. Samaddar, Phys. Rev. C **85**, 024310 (2012).
[44] M. K. Gaidarov, A. N. Antonov, P. Sarriguren, and E. Moya de Guerra, Phys. Rev. C **84**, 034316 (2011).
[45] A. N. Antonov, V. A. Nikolaev, and I. Zh. Petkov, Bulg. J. Phys. **6**, 151 (1979); Z. Phys. A **297**, 257 (1980); Nuovo Cimento A **86**, 23 (1985); A. N. Antonov, E. N. Nikolov, I. Zh. Petkov, C. V. Christov, and P. E. Hodgson, *ibid.* **102**, 1701 (1989); A. N. Antonov, D. N. Kadrev, and P. E. Hodgson, Phys. Rev. C **50**, 164 (1994).
[46] A. N. Antonov, V. A. Nikolaev, and I. Zh. Petkov, Z. Phys. A **304**, 239 (1982).
[47] M. K. Gaidarov, A. N. Antonov, P. Sarriguren, and E. M. de Guerra, Phys. Rev. C **85**, 064319 (2012).
[48] K. A. Brueckner, J. R. Buchler, S. Jorna, and R. J. Lombard, Phys. Rev. **171**, 1188 (1968).
[49] K. A. Brueckner, J. R. Buchler, R. C. Clark, and R. J. Lombard, Phys. Rev. **181**, 1543 (1969).
[50] A. N. Antonov, P. E. Hodgson, and I. Zh. Petkov, *Nucleon Momentum and Density Distributions in Nuclei* (Clarendon, Oxford, 1988); *Nucleon Correlations in Nuclei* (Springer, Berlin, 1993).
[51] M. Bhuyan, B. V. Carlson, S. K. Patra, and S.-G. Zhou, Phys. Rev. C **97**, 024322 (2018).
[52] J. N. De, X. Viñas, S. K. Patra, and M. Centelles, Phys. Rev. C **64**, 057306 (2001).
[53] S. K. Samaddar, J. N. De, X. Viñas, and M. Centelles, Phys. Rev. C **75**, 054608 (2007).
[54] B. K. Agrawal, D. Bandyopadhyay, J. N. De, and S. K. Samaddar, Phys. Rev. C **89**, 044320 (2014).
[55] Z. W. Zhang, S. S. Bao, J. N. Hu, and H. Shen, Phys. Rev. C **90**, 054302 (2014).
[56] R. J. Furnstahl, B. D. Serot, and H. B. Tang, Nucl. Phys. A **598**, 539 (1996); **615**, 441 (1997).

[57] R. Lisboa, M. Malheiro, and B. V. Carlson, Phys. Rev. C **93**, 024321 (2016).
[58] Y. K. Gambhir, J. P. Maharana, G. A. Lalazissis, C. P. Panos, and P. Ring, Phys. Rev. C **62**, 054610 (2000).
[59] S. S. Avancini, M. E. Bracco, M. Chiapparini, and D. P. Menezes, Phys. Rev. C **67**, 024301 (2003).
[60] Y. F. Niu, Z. M. Niu, N. Paar, D. Vretenar, G. H. Wang, J. S. Bai, and J. Meng, Phys. Rev. C **88**, 034308 (2013).
[61] S. K. Singh, S. K. Biswal, M. Bhuyan, and S. K. Patra, Phys. Rev. C **89**, 044001 (2014).
[62] N. Alam, H. Pais, C. Providência, and B. K. Agrawal, Phys. Rev. C **95**, 055808 (2017).
[63] O. Lourenco, M. Dutra, and D. P. Menezes, Phys. Rev. C **95**, 065212 (2017).
[64] M. Centelles, X. Viñas, M. Barranco, and P. Shuck, Ann. Phys. (NY) **221**, 165 (1993).
[65] E. Wigner, Phys. Rev. **40**, 749 (1932).
[66] J. G. Kirkwood, Phys. Rev. **44**, 31 (1933).
[67] M. Brack, G. Guet, and H. B. Hakansson, Phys. Rep. **123**, 275 (1985).
[68] M. Centelles, X. Viñas, M. Barranco, N. Ohtsuka, A. Faessler, D. T. Khoa, and H. Müther, J. Phys. G **17L**, 193 (1991).
[69] S. K. Samaddar, J. N. De, X. Viñas, and M. Centelles, Phys. Rev. C **78**, 034607 (2008).
[70] E. Moya de Guerra, P. Sarriguren, J. A. Caballero, M. Casas, and D. W. L. Sprung, Nucl. Phys. A **529**, 68 (1991).
[71] W.-C. Chen and J. Piekarewicz, Phys. Lett. B **748**, 284 (2015).
[72] G. A. Lalazissis, J. König, and P. Ring, Phys. Rev. C **55**, 540 (1997).
[73] M. Wang, G. Audi, A. H. Wapstra, F. G. Kondev, M. MacCormick, X. Xu, and B. Pfeiffer, Chin. Phys. C **36**, 1603 (2012).
[74] I. Angeli and K. P. Marinova, At. Data Nucl. Data Tables **99**, 69 (2013).
[75] K. Hebeler, J. M. Lattimer, C. J. Pethick, and A. Schwenk, Astrophys. J. **773**, 11 (2013).
[76] G. Q. Li, R. Machleidt, and R. Brockmann, Phys. Rev. C **45**, 2782 (1992).
[77] M. Baldo and C. Maieron, Phys. Rev. C **77**, 015801 (2008).
[78] P. Danielewicz, R. Lacey, and W. G. Lynch, Science **298**, 1592 (2002).
[79] H.-Th. Janka, K. Langanke, A. Marek, G. Martinez-Pinedo, and B. Müller, Phys. Rep. **442**, 38 (2007)
[80] Y. Zhu and J.C. Pei, Phys. Rev. C **90**, 054316 (2014).